Using wind observations from nearby aircraft to update the optimal descent trajectory in real-time

Ramon Dalmau and Xavier Prats
Department of Physics - Aeronautics Division
Technical University of Catalonia – BarcelonaTECH
Castelldefels, Barcelona, Spain

Brian Baxley
Crew Systems and Aviation Operations Branch
NASA Langley Research Center (LaRC)
Hampton, VA, USA

***Abstract*—The ability to meet a controlled time of arrival during a continuous descent operation will enable environmentally friendly and fuel efficient descent operations while simultaneously maintaining airport throughput. However, if the wind forecast used to compute the initial trajectory plan is not accurate enough, the guidance system will need to correct time deviations from the plan during the execution of the descent. Previous work proposed an on-board guidance strategy based on model predictive control, which repeatedly updates the trajectory plan in real-time from the current aircraft state and for the remainder of the descent. However, the wind conditions downstream, at altitudes not explored yet, were difficult to predict due to the lack of data. This paper shows the potential benefits of using wind observations, broadcast by nearby aircraft, to reconstruct the wind profile downstream. The wind profile in the trajectory optimization problem is modeled as a spline, which control points are updated to fit the observations before re-planning the trajectory. Results from simulations using realistic wind data show that the performance of model predictive control significantly improves when including up-to-date wind observations, in terms of time and energy errors at the metering fix and fuel consumption.**

I. Introduction

Continuous descent operations (CDOs) with controlled times of arrival (CTAs) at metering fixes could enable more environmentally friendly procedures while simultaneously maintaining (or even increasing) airport and airspace throughput.

These type of time-based flight operations are a cornerstone for the queue-management project by the Single European Sky Air traffic management Research (SESAR) program in Europe, and for the analogous Time-Based Flow Management (TBFM) program in the United States. One of the goals of both projects is to use timing at meter points to more efficiently deliver aircraft to the terminal maneuvering area.

The RTCA published standards for time of arrival control as 95% compliance with accuracy levels of ± 10 s for CTAs involving descents subject to the wind uncertainty model described in [1]. In this context, several studies investigated the effect of errors in the wind forecast on the performance of CDOs with CTAs [2], [3], and concluded that an accurate knowledge of the actual wind conditions is of utmost importance. Results from a flight test conducted at the Denver International Airport (KDEN) that explored seven different categories of errors in trajectory calculations by the flight management systems (FMSs), indicated that approximately two-thirds of the mean time error and nearly all of the standard deviation was due to an incorrect wind forecast [4]. Other flight trials described in Ref. [5], also showed the importance of using a high-quality wind forecast during the trajectory planning process to accurately comply with CTAs.

State-of-the-art FMSs compute the optimal descent trajectory plan satisfying applicable CTAs before starting the descent, using the best available forecast of the wind along the route towards the arrival airport. Then, this initial trajectory is *frozen* and the guidance system uses different strategies to execute it. However, the initial trajectory plan shows only what can be achieved given perfect knowledge of the actual wind conditions. If the wind forecast used by the FMS does not match the actual wind conditions, the initial trajectory plan is no longer the most optimal, and some operational constraints (including the CTA) may be violated if errors are not actively nullified by the guidance system. The use of accurate and up-to-date wind data when planning the initial trajectory could potentially reduce the throttle and speed brakes actions commanded by the guidance system and to significantly improve compliance with CTAs. Moreover, a primary driver of accurate CTA compliance is not only the quality of the wind forecast provided to the FMS, but also the guidance strategy used to execute the trajectory plan [6].

Previous work [7] showed that nonlinear model predictive control (NMPC) [8], is very robust in terms of correcting energy (speed and altitude) and time deviations, providing at the same time acceptable fuel consumption and noise nuisance figures. NMPC is a guidance strategy based on a frequent update of the optimal trajectory plan during the execution of the descent. Other research [9] has also demonstrated the feasibility of using NMPC to achieve precise spacing between aircraft, the objective of interval management (IM) operations.

Recently, the NMPC guidance algorithm was enhanced to enable the calculation of the optimal trajectory plan using a wind profile based on the original forecast but progressively updated based on the ownship sensed winds [10]. However, that only corrects the wind profile for current and previous positions, not *downstream* positions, that is, from current position to destination. The short-coming of using ownship sensed winds is that any time deviation due to an incorrect wind forecast at a downstream waypoint requires a higher and higher change to the aircraft's airspeed as the distance to that point becomes shorter and shorter [6]. Using wind observations from

aircraft that have recently crossed downstream waypoints at an altitude similar to that planned by the ownship is expected to improve the accuracy of the ownship trajectory prediction that is essential to meeting any constraints and CTAs.

Refs. [11]–[13] proposed wind prediction algorithms that use wind observations broadcast by nearby aircraft to update, on-board and in real-time, the wind profile used to calculate the trajectory plan. Other studies investigating aircraft spacing during IM operations showed that the use of wind predictions generated from observations emitted by aircraft in range within a *wind networking* concept could reduce the spacing time error if compared with using outdated wind information [14].

In this paper, the NMPC guidance strategy is implemented to guide aircraft during CDOs subject to CTAs, and uses the concept of accessing data available in a hypothetical wind networked environment to generate accurate and up-to-date wind predictions on-board and in real-time.

II. Background

This paper assesses the benefit of combining a NMPC guidance strategy with updating the wind profile using wind observations broadcasted by nearby aircraft.

A. Nonlinear model predictive control (NMPC)

NMPC is based on the solution, at each time sample, of an optimal control problem over a future time horizon [8]. The resulting optimal control is applied only until the next time sample, where the optimal control problem is solved again.

Typical NMPC applications consider a fixed-length time horizon, which advances an interval sample at each recalculation. Alternatively, when the system has to reach a certain state at a particular time, a shrinking horizon is often preferred. Using this strategy, the length of the horizon is not fixed but decreases by one interval sample at each trajectory update.

1) NMPC trajectory optimization: Many *real-life* processes, such as the descent of an aircraft, can be divided into several phases (or stages) where the dynamics of the system, the cost function and/or the constraints might change. Note that, in this paper, the term *phase* does not refer to the standard phases of a flight (e.g., take-off, climb, cruise), but to the stages of a generic multi-phase optimal control problem.

Let the continuous time horizon $[t_I, t_F]$ be divided into P time intervals $[t_j, t_{j+1}]$ for $j = 0, \ldots, P-1$, where each time interval corresponds to a different phase. Note that $t_0 = t_I$ and $t_P = t_F$. Then, each time intervals (phase) is discretized into N_j equidistant time samples $\tau_k, \tau_{k+1}, \ldots, \tau_{k+N_j-1}$, where $\tau_k = t_j$, $\tau_{k+N_j-1} = t_{j+1}$ and $k = \sum_{i<j} N_i$, for all $j = 0, \ldots, P-1$. The discretization step of the j^{th} phase is denoted by $\Delta\tau_j$. As a result, the whole time horizon is discretized into $N+1 = \sum_{j=0}^{P-1} N_j$ time samples $\tau_0, \tau_1, \ldots, \tau_N$.

Let $\mathcal{T}$ be a multi-dimensional set that relates the index of each phase to the indexes of its corresponding time samples. The subset $\mathcal{E} \subseteq \mathcal{T}$ only includes the index corresponding to the last time sample of each phase; and $\mathcal{I}$ is defined as $\mathcal{T} \backslash \mathcal{E}$.

The optimal control problem starting at τ_0, and minimizing a cost function J in the remaining time horizon is:

$$
\begin{aligned}
\min_{\substack{\boldsymbol{x}_k, k=0,\ldots,N \\ \boldsymbol{u}_k, k=0,\ldots,N-1}} \quad & J := \sum_{(j,k)\in\mathcal{E}} \phi_j\left(\boldsymbol{x}_k, \boldsymbol{d}\right) + \sum_{(j,k)\in\mathcal{I}} \Pi_j\left(\boldsymbol{x}_k, \boldsymbol{u}_k, \boldsymbol{d}, \Delta\tau_j\right) \\
\text{s.t} \quad & \boldsymbol{x}_0 = \boldsymbol{X} \\
& \boldsymbol{x}_{k+1} = \boldsymbol{F}_j\left(\boldsymbol{x}_k, \boldsymbol{u}_k, \boldsymbol{d}, \Delta\tau_j\right); \forall (j,k) \in \mathcal{I} \\
& \boldsymbol{b}_j^{eq}\left(\boldsymbol{x}_k, \boldsymbol{u}_k, \boldsymbol{d}\right) = 0; \forall (j,k) \in \mathcal{I} \\
& \boldsymbol{b}_j^{in}\left(\boldsymbol{x}_k, \boldsymbol{u}_k, \boldsymbol{d}\right) \leq 0; \forall (j,k) \in \mathcal{I} \\
& \boldsymbol{\vartheta}_j^{eq}\left(\boldsymbol{x}_k, \boldsymbol{d}\right) = 0; \forall (j,k) \in \mathcal{E} \backslash \{(P-1, N)\} \\
& \boldsymbol{\vartheta}_j^{in}\left(\boldsymbol{x}_k, \boldsymbol{d}\right) \leq 0; \forall (j,k) \in \mathcal{E} \backslash \{(P-1, N)\} \\
& \boldsymbol{\psi}\left(\boldsymbol{x}_N, \boldsymbol{d}\right) = 0 \\
& \boldsymbol{x}_k - \boldsymbol{x}_{k+1} = 0; \forall (j,k) \in \mathcal{E} \backslash \{(P-1, N)\},
\end{aligned}
\tag{1}
$$

where $\boldsymbol{x}_k \in \Re^{n_x}$ and $\boldsymbol{u}_k \in \Re^{n_u}$ are the state and control vectors discretized at τ_k, respectively; $\boldsymbol{d} \in \Re^{n_d}$ is the vector of fixed parameters of the model; $\boldsymbol{b}_j^{eq} : \Re^{n_x} \times \Re^{n_u} \times \Re^{n_d} \to \Re^{n_{\varphi_j}}$ and $\boldsymbol{b}_j^{in} : \Re^{n_x} \times \Re^{n_u} \times \Re^{n_d} \to \Re^{n_{b_j}}$ are the algebraic and path constraints, respectively, of the j^{th} phase; $\boldsymbol{\vartheta}_j^{eq} : \Re^{n_x} \times \Re^{n_d} \to \Re^{n_{\vartheta_j^{eq}}}$ and $\boldsymbol{\vartheta}_j^{in} : \Re^{n_x} \times \Re^{n_d} \to \Re^{n_{\vartheta_j^{in}}}$ represent applicable equality and inequality interior-point constraints, respectively, applied at the last time of the j^{th} phase; $\boldsymbol{\psi} : \Re^{n_x} \times \Re^{n_d} \to \Re^{n_\psi}$ are the terminal constraints; and $\Pi_j : \Re^{n_x} \times \Re^{n_u} \times \Re^{n_d} \times \Re \to \Re$ and $\boldsymbol{F}_j : \Re^{n_x} \times \Re^{n_u} \times \Re^{n_d} \times \Re \to \Re^{n_x}$ are the quadrature and states evolution functions for the j^{th} phase, respectively, which are the result of integrating the continuous running cost (π_j) and the system ordinary differential equations (ODEs) describing the dynamics of the system ($\boldsymbol{f}_j$) during an interval of duration $\Delta\tau$ using the discretized states and controls. For instance, using the Euler method, these functions would be:

$$
\boldsymbol{F}_j(\boldsymbol{x}_k, \boldsymbol{u}_k, \boldsymbol{d}, \Delta\tau_j) = \boldsymbol{x}_k + \boldsymbol{f}_j\left(\boldsymbol{x}_k, \boldsymbol{u}_k, \boldsymbol{d}\right) \Delta\tau_j, \tag{2a}
$$

$$
\Pi_j(\boldsymbol{x}_k, \boldsymbol{u}_k, \boldsymbol{d}, \Delta\tau_j) = \pi_j\left(\boldsymbol{x}_k, \boldsymbol{u}_k, \boldsymbol{d}\right) \Delta\tau_j; \forall (j,k) \in \mathcal{I}. \tag{2b}
$$

Note that the discretization step of each individual phase could be considered either a known parameter or variable to be optimized, depending on the context. For instance, if the duration of the whole time horizon were fixed to a certain parameter, say a CTA, but the duration of each phase were flexible, $\Delta\tau_j$ for $j = 0, \ldots, P-1$ would become additional decision variables subject to the following constraint:

$$
\sum_{j=0}^{P-1} \left(N_j - 1\right) \Delta\tau_j - \text{CTA} = 0, \tag{3}
$$

which would be appended to Eq. (1).

The optimal trajectory plan can be computed by formulating the discrete-time optimal control problem Eq. (1) as the following parametric nonlinear programming (NLP) problem:

$$
\begin{aligned}
\min_{\boldsymbol{z}} \quad & f\left(\boldsymbol{z}, \boldsymbol{p}\right) \\
\text{s.t} \quad & \boldsymbol{h}\left(\boldsymbol{z}, \boldsymbol{p}\right) = 0 \\
& \boldsymbol{g}\left(\boldsymbol{z}, \boldsymbol{p}\right) \leq 0,
\end{aligned}
\tag{4}
$$

where $\boldsymbol{z} \in \Re^{n_z}$ is the vector of primal variables; $\boldsymbol{h} : \Re^{n_z} \times \Re^{n_p} \rightarrow \Re^{n_h}$ and $\boldsymbol{g} : \Re^{n_z} \times \Re^{n_p} \rightarrow \Re^{n_g}$ are the vectors of equality and inequality constraints, respectively; and $\boldsymbol{p} \in \Re^{n_p}$ is the vector of (fixed) parameters of the NLP optimization problem. In this paper, the following notation has been used:

$$\begin{aligned} \boldsymbol{z} &:= [\boldsymbol{z}_0, \boldsymbol{z}_1, \ldots, \boldsymbol{z}_N]^T \\ \boldsymbol{h}(\boldsymbol{z}, \boldsymbol{p}) &:= [\boldsymbol{h}_0(\boldsymbol{z}, \boldsymbol{p}), \boldsymbol{h}_1(\boldsymbol{z}, \boldsymbol{p}), \ldots, \boldsymbol{h}_N(\boldsymbol{z}, \boldsymbol{p})]^T \\ \boldsymbol{g}(\boldsymbol{z}, \boldsymbol{p}) &:= [\boldsymbol{g}_0(\boldsymbol{z}, \boldsymbol{p}), \boldsymbol{g}_1(\boldsymbol{z}, \boldsymbol{p}), \ldots, \boldsymbol{g}_N(\boldsymbol{z}, \boldsymbol{p})]^T, \end{aligned} \tag{5}$$

where $(\cdot)^T$ represents the transpose of $(\cdot)$ and

$$\begin{aligned} \boldsymbol{z}_k &:= \begin{cases} [\boldsymbol{u}_k, \boldsymbol{x}_k]^T & \text{if } k \neq N \\ \boldsymbol{x}_k & \text{if } k = N \end{cases} \\ \boldsymbol{h}_k &:= \begin{cases} \left[\boldsymbol{x}_{k+1} - \boldsymbol{F}_{j,k}, \boldsymbol{b}_{j,k}^{eq}\right]^T & \text{if } (j,k) \in \mathcal{I} \\ \left[\boldsymbol{\vartheta}_{j,k}^{eq}, \boldsymbol{x}_k - \boldsymbol{x}_{k+1}\right]^T & \text{if } (j,k) \in \mathcal{E} \backslash \{P-1, N\} \\ \boldsymbol{\psi}(\boldsymbol{x}_k, \boldsymbol{d}) & \text{if } k = N \end{cases} \\ \boldsymbol{g}_k &:= \begin{cases} \boldsymbol{b}_{j,k}^{in} & \text{if } (j,k) \in \mathcal{I} \\ \boldsymbol{\vartheta}_{j,k}^{in} & \text{if } (j,k) \in \mathcal{E} \backslash \{P-1, N\}. \end{cases} \end{aligned} \tag{6}$$

According to Eq. (6), $\boldsymbol{z}_k$ includes both discretized states and controls at the time sample τ_k. Similarly, $\boldsymbol{g}_k$ and $\boldsymbol{h}_k$ include the inequality and equality constraints applied at τ_k.

In Eq. (4), f is the cost function of the original optimal control problem evaluated at the primal variables and fixed NLP parameters, i.e., $f(\boldsymbol{z}, \boldsymbol{p}) = J(\boldsymbol{z}, \boldsymbol{p})$. In this paper, the vector of fixed NLP parameters is composed of the initial conditions ($\boldsymbol{X}$) and the parameters of the model, i.e., $\boldsymbol{p} = [\boldsymbol{X}, \boldsymbol{d}]^T$.

Furthermore, in order to reduce the number of variables and constraints, the constraint that determines the initial condition of the optimal control problem to the current state of the system is eliminated by substituting the variables $\boldsymbol{x}_0$ for the initial conditions $\boldsymbol{X}$ in the whole NLP optimization problem. This makes the constraint $\boldsymbol{x}_0 = \boldsymbol{X}$ of Eq. (1) redundant, allowing to remove the variable $\boldsymbol{x}_0$ from the calculations.

Let $\mathcal{P}_N$ be the NLP algorithm that provides the optimal primal-dual solution as a function of $\boldsymbol{p}$ for the next N samples:

$$(\boldsymbol{z}^*, \boldsymbol{\lambda}^*, \boldsymbol{\mu}^*) \leftarrow \mathcal{P}_N(\boldsymbol{p}) \tag{7}$$

where $\boldsymbol{\lambda} \in \Re^{n_g}$ and $\boldsymbol{\mu} \in \Re^{n_h}$ are the Lagrange multipliers (dual variables) paired up with the constraints $\boldsymbol{g}$ and $\boldsymbol{h}$, respectively. A more technical description of the conditions necessary for optimality is found in Ref. [10].

When using the shrinking horizon NMPC, the optimal control problem is solved at each τ_i, $i = 0, \ldots, N-1$ in order to obtain the optimal trajectory starting at τ_i and extending to τ_N. Let $\mathcal{P}_{N-i}$ be the NLP algorithm that provides the optimal primal-dual solution as a function of $\boldsymbol{p}$, but starting at τ_i:

$$(\boldsymbol{z}_{i:}^*, \boldsymbol{\lambda}_{i:}^*, \boldsymbol{\mu}_{i:}^*) \leftarrow \mathcal{P}_{N-i}(\boldsymbol{p}) \tag{8}$$

where $(\cdot)_{i:}$ indicates the elements of $(\cdot)$ corresponding to time samples from τ_i to the end of the time horizon (τ_N).

2) NMPC guidance strategy: In an ideal case, problem $\mathcal{P}_{N-i}$ is solved at each τ_i, as soon as the parameter vector $\boldsymbol{p}$ is measured or estimated. Then, the resulting optimal control $\boldsymbol{u}_i^*$ is applied without delay until τ_{i+1}, where the process is repeated. However, for achieving optimal performance and good stability properties, problem $\mathcal{P}_{N-i}$ needs to be solved instantaneously. We refer to this hypothetical case as the ideal NMPC (INMPC). Algorithm 1 details its main steps.

Algorithm 1 Ideal NMPC (INMPC)

1: $(\boldsymbol{z}_{0:}^*, \boldsymbol{\lambda}_{0:}^*, \boldsymbol{\mu}_{0:}^*) \leftarrow \mathcal{P}_N(\boldsymbol{p})$
2: **for** $i = 1, \ldots, N-1$ **do**
3: Measure $\boldsymbol{X}$ and estimate $\boldsymbol{d}$
4: $\boldsymbol{p} \leftarrow [\boldsymbol{X}, \boldsymbol{d}]^T$
5: $(\boldsymbol{z}_{i:}^*, \boldsymbol{\lambda}_{i:}^*, \boldsymbol{\mu}_{i:}^*) \leftarrow \mathcal{P}_{N-i}(\boldsymbol{p})$
6: Implement $\boldsymbol{u}_i^*$ until τ_{i+1}

In practical applications $\mathcal{P}_{N-i}$ may be computationally expensive to solve. This implies that the control $\boldsymbol{u}_i^*$ cannot be applied just after $\boldsymbol{p}$ is measured or estimated, but only after $\mathcal{P}_{N-i}$ is solved. The delay in calculating the new solution may lead to sub-optimum trajectories, failure to meet constraints, or in some instances instabilities of the solution [15]. This motivates the introduction of sensitivity-based methods, which rapidly update the optimal descent trajectory plan by using parametric sensitivities instead of solving a rigorous NLP optimization problem at each time sample.

Previous work [10] showed that the performance of sensitivity-based methods are similar to those of the INMPC, with the sensitivity-based methods being simpler, faster and more robust. Since the performance was similar, it is expected that the results from the addition of *wind networking* to the INMPC guidance strategy described in this paper should also apply to the sensitivity-based methods.

B. Wind sources and models

The accuracy of a trajectory plan computed by the FMS, especially the computation of the estimated time of arrival, critically depends on the quality of the wind forecast [4].

Section II-B1 describes the sources of weather data and the wind models used by state-of-the-art FMSs to generate the trajectory plan. Section II-B2 presents basic concepts of wind networking and lists some relevant works on this topic.

1) Conventional wind sources and models: Currently, the flight crew receives the wind forecast from the flight dispatcher and either enters that information manually into the FMS or automatically via a data communication system.

The typical FMS allows for storing the forecast wind value at each departure and arrival waypoint, and up to five values for each en route waypoint. Operationally, the five altitudes are usually above, at, and below the aircraft's expected altitude, allowing the FMS to interpolate between the altitudes. When required, the FMS can also extrapolate beyond those altitudes or limits to perform trajectory predictions.

The wind data entered to the FMS are primarily based on wind charts from numerical weather prediction (NWP) models.

Nowadays, the observations required to initialize NWP models are mainly gathered from radiosondes and aircraft equipped with AMDAR (aircraft meteorological data relay). However, the spatial distribution of the radiosondes, which are launched only two to four times a day, is too coarse, and wind observations gathered through AMDAR are not sufficient because not all aircraft in operation are equipped with that system [16].

Due to the relatively low spatio-temporal resolution of the data used to initialize NWP models and the computational burden of running a prediction, wind forecasts are generated only three to eight times per day, and are valid until +6, +12 or +24 hours beyond their issued time. Consequently, the wind forecast for the descent is not tailored for the current as-amended flight plan, and could be several hours old by the time the top of descent (TOD) is reached.

Most flight planning suppliers currently use the world area forecast model that is produced to an ICAO specification by meteorological providers. Some flight plan supplies also generate their own wind forecasts at a finer resolution, but do not provide a higher update rate due to the time required to uplink the data to the FMS using the available bandwidth [17].

2) Wind networking: Aircraft could be used as a network of airborne sensors emitting the sensed wind to ground systems [18] or to nearby aircraft [19] to provide accurate, high-resolution and up-to-date wind data replacing or complementing the forecasts obtained from NWP models. At present, however, aircraft rarely broadcast this valuable information.

Fortunately, the wind vector can be indirectly inferred from standard surveillance data already in place. Several works already proposed to use wind observations derived from surveillance data to provide enhanced wind predictions for the air traffic management (ATM) community. Most wind estimation methods found in the literature rely on the fact that the wind vector is the difference between the ground speed vector and the true airspeed (TAS) vector.

Early in the 1980s, Ref. [18] was the first to propose a method to estimate the wind vector from ground-based (radar) surveillance observations. The ground speed vectors for every scan of each aircraft track were obtained by taking the difference between the sequential radar positions of aircraft and then dividing by the scan interval. Then, the ground speed vectors from multiple aircraft were used to infer the wind vector by means of Bayesian estimation techniques, assuming constant wind speed and aircraft airspeed during turning maneuvers. An extension of this algorithm was investigated in [20].

Aircraft equipped with Advanced Surveillance-Broadcast (ADS-B) autonomously transmit surveillance data including not only aircraft position but also ground speed vector. The wide availability of ADS-B receivers at a relatively low cost and the growing amount of aircraft equipped with this surveillance system make ADS-B an attractive source of data for many ATM applications. Similarly to Refs. [18] and [20], Ref. [19] proposed a method to estimate the wind vector from ground speed vector observations. In this case, however, the ground speed vector was directly obtained from the ADS-B surveillance messages. The method was based on a modified extended Kalman filter that estimates the wind recursively from an aircraft in a turn. In addition, a new method to estimate wind using data from multiple aircraft was also proposed.

Mode-S messages emitted by the aircraft surveillance system as a response to a secondary surveillance radar interrogation includes information about the ground speed and TAS vector, from which the wind vector can be directly inferred. The use of Mode-S data for wind networking applications was investigated in [21]. Recently, Ref. [22] applied geostatistical techniques to generate a four-dimensional wind model for the terminal maneuvering area; and Ref. [23] investigated a novel and relatively fast gas particle model that estimates the wind field in real-time from ADS-B and Mode-S messages.

In summary, the capability to derive the sensed wind data from aircraft transmitting ADS-B and Mode-S messages will provide the FMS more accurate information from which to calculate the optimum trajectory. Nearby aircraft, in particular those on the same trajectory, broadcast data that can be used to update and improve the wind profile used by the FMS to optimize the trajectory while meeting constraints and CTAs.

III. NMPC GUIDANCE STRATEGY FOR A TIME-CONSTRAINED CDO

In this Section the generic optimal control Eq. (1) problem is particularized for an aircraft already in descent on a CDO that is subject to a time constraint at a single metering fix. Then, an algorithm to estimate the wind profile is proposed.

A. Optimal control problem formulation

The state vector $\boldsymbol{x} = [t, v, h]^T$ is composed of time, TAS, and altitude; the control vector $\boldsymbol{u} = [\gamma, T, \beta]^T$ is composed of the aerodynamic flight path angle, engine thrust, and speed brakes deflection. The flight path angle is the control that is used by the aircraft to modulate energy (i.e., exchange potential energy for kinetic energy and vice-versa), whereas thrust and speed brakes are used to add and remove energy.

Different from typical approaches, the independent variable is the distance to go (s) and not the time. The selection of s as the independent variable is driven by the fact that during an ideal CDO, with no intervention from the air traffic controllers (ATC) except for the assignment of the CTA, the aircraft will follow a *closed-loop* route and the remaining distance to go will be known. In addition, this formulation replicates how constraints are defined in the current operational environment, thereby enabling more precise modeling of the constraints.

For the remainder of this document the optimal control problem will be formulated in the continuous domain aiming to keep the notation simple. However, the problem needs to be discretized in the form of Eq. (1).

The dynamics of $\boldsymbol{x}$ are expressed by the following ODEs, considering a point-mass representation of the aircraft reduced to a gamma-command model, where vertical equilibrium is assumed and the cross and vertical winds are assumed negligible:

$$\boldsymbol{f}_j = \frac{\mathrm{d}\boldsymbol{x}}{\mathrm{d}s} = \begin{bmatrix} 1 \\ \frac{T - D(v,h,\beta)}{m} - g\sin\gamma \\ v\sin\gamma \end{bmatrix} \frac{1}{v\cos\gamma + w(h)} \quad (9)$$

where $D : \mathbb{R}^{n_x \times n_u} \to \mathbb{R}$ is the aerodynamic drag; g is the gravity acceleration; m is the mass, which is assumed to be constant since the fuel consumption during a descent is a small fraction of the total mass [24]; and the longitudinal component of the wind $w : \mathbb{R} \to \mathbb{R}$ is modeled by a smoothing spline [25]:

$$w(h) = \sum_{i=1}^{n_c} c_i B_i(h) \quad (10)$$

where B_i, $i = 1, \ldots, n_c$, are the B-spline basis functions and $\boldsymbol{c} = [c_1, \ldots, c_{n_c}]$ are control points of the smoothing spline. It should be noted that the longitudinal wind has been modeled as a function of the altitude only, as done in similar works [12].

The goal is to minimize a weighted sum of the fuel consumption and speed brakes use (which leads to airframe noise) for the remaining descent. Thus, the running cost is:

$$\pi_j = \frac{q(v,h,T) + K_\beta \beta}{(v\cos\gamma + w(h))} \quad (11)$$

where $q : \mathbb{R}^{n_x \times n_u} \to \mathbb{R}$ is the fuel flow and K_β a parameter that determines how much the use of speed brakes is penalized.

Furthermore, generic phase-independent path constraints on the controls ensure that the maximum and minimum descent gradients, thrust and speed brakes are not exceeded throughout the descent: $\boldsymbol{b}^{in} = \left[\gamma, \gamma_{min} - \gamma, T_{min} - T, T - T_{max}, -\beta, \beta - 1\right]^T$, where γ_{min} is the maximum descent gradient; $T_{min} : \mathbb{R}^{n_x} \to \mathbb{R}$ and $T_{max} : \mathbb{R}^{n_x} \to \mathbb{R}$ are the idle and maximum thrust, respectively; $\beta = 0$ and $\beta = 1$ indicate that speed brakes are retracted and fully extended.

Different alternatives can be used to model the aircraft performance functions T_{min}, T_{max}, D and q and their respective parameters. In this paper, the EUROCONTROL's base of aircraft data (BADA) v4 model has been adopted [26]. However, BADA v4 does not include a model for the effects of the speed brakes on the drag coefficient (C_D). As a workaround, in this paper the contribution of the speed brakes is modeled as an extra linear term $C_{D_\beta}\beta$ in the generic BADA v4 drag coefficient model, where C_{D_β} is a coefficient representing the increase in drag coefficient for unit of speed brakes deflection.

Terminal constraints fix the state vector at the metering fix:

$$\boldsymbol{\psi} = \begin{bmatrix} t - \mathrm{CTA} \\ v_{CAS}(h,v) - v_{CAS_F} \\ h - h_F \end{bmatrix} \quad (12)$$

where $v_{CAS} : \mathbb{R}^{n_x} \to \mathbb{R}$ is the calibrated airspeed (CAS); v_{CAS_F} and h_F are the CAS and altitude at the metering fix.

The vector of model parameters includes the control points of the spline approximating the longitudinal wind and the CTA, i.e., $\boldsymbol{d} = [\boldsymbol{c}, \mathrm{CTA}]^T$. This definition allows the optimal trajectory to be updated whenever an improved wind forecast is available or the CTA is tactically modified by ATC.

Finally, the descent is divided into P phases, defined between two consecutive waypoints of the lateral route with associated speed and/or altitude constraints. In each phase, the different operational constraints that may apply can be modeled in the form of path, algebraic and/or interior-point constraints. The exact number of phases and associated constraints depend on the particular procedure being investigated.

B. Update of wind profile

Given a set $\mathcal{O}$ composed by n_o wind observations with associated time stamps $(\hat{h}_k, \hat{w}_k, \tau_k)$, $k = 1, \ldots, n_o$, and a vector of fixed knots, the optimal location of the control points $c_k, k = 1, \ldots, n_c$, that minimize the curvature of the smoothing spline while bounding the approximation error is obtained by solving a weighted least-squares fitting problem:

$$\begin{aligned} \min_{c_k, k=1,\ldots,n_c} \quad & \int w''(h)^2 \mathrm{d}h \\ \text{s.t} \quad & \sum_{k=1}^{n_o} \omega_k \left(w(\hat{h}_k) - \hat{w}_k \right)^2 \leq \varepsilon \end{aligned} \quad (13)$$

where ε specifies the trade-off between smoothness and accuracy of the approximation. The weights associated with the observations can be defined in many different ways. In this paper, the weights are updated at each time sample τ_i according to $\omega_k = \Lambda^{\tau_k - \tau_i}$, where τ_k is the time sample when the observation at $\hat{h}_k$ was obtained, regardless of the source of information and its geographical location. The forgetting factor $\Lambda \in [0, 1]$ weights the more recent measurements so that old observations are discounted at an exponential rate.

IV. Experiment setup

A 1x5 test matrix was used to assess the benefits of combining wind estimation and NMPC guidance along a CDO. The CDO selected is currently in use at KDEN, and a subset of altitude and speed constraints at four waypoints were modeled. Within each of the five cells of the text matrix, the CDO was flown 10 times, with each repetition using an initial forecast wind profile and an actual wind profile to generate wind error for the aircraft model to experience. The same set of 10 actual wind profiles was used in each test cell to create identical wind error per run, allowing direct comparison of results by run.

A. Arrival route

The BOSSS TWO standard arrival procedure at KDEN was selected as the starting point to define the lateral route and the vertical profile used in this paper. The metering fix where CTAs were assigned by an hypothetical ATC during the simulations was the final approach point (DYMON). A more detailed view of this procedure can be found in [10].

From all the waypoints of the route, only the altitude and speed constraints at QUAIL, BOSSS, CHAPP and DYMON were modeled. In order to accomplish that, the descent was

divided in $P = 4$ different phases, with associated phase-dependent path, algebraic and/or interior-point constraints. It should be noted, however, that the fact of modeling few constraints of the real procedure is not a shortcoming nor a limitation of the model. The model proposed in this paper can handle an unlimited number of phases and associated constraints, yet few constraints have been selected aiming to represent a futuristic and less restricted procedure facilitating CDOs, as well as to ease the interpretation of the results. Table I wraps up the different phases and constraints.

TABLE I
PHASES AND ASSOCIATED CONSTRAINTS FOR THE BOSSS TWO

Phase	$\boldsymbol{b}_j^{in}$	$\boldsymbol{\varphi}_j^{eq}$	$\boldsymbol{\vartheta}_j^{in}$	$\boldsymbol{\vartheta}_j^{eq}$
0	$\begin{bmatrix} M - \text{MMO} \\ v_{CAS} - \text{VMO} \\ 250\,\text{kt} - v_{CAS} \end{bmatrix}$	-	$\begin{bmatrix} \text{FL170} - h \\ h - \text{FL190} \end{bmatrix}$	$\begin{bmatrix} v_{CAS} - 250\,\text{kt} \end{bmatrix}$
1	$\begin{bmatrix} v_{CAS} - 250\,\text{kt} \\ 210\,\text{kt} - v_{CAS} \end{bmatrix}$	-	-	$\begin{bmatrix} v_{CAS} - 210\,\text{kt} \\ h - 12,000\,\text{ft} \end{bmatrix}$
2	$\begin{bmatrix} v_{CAS} - 210\,\text{kt} \\ \text{GD} - v_{CAS} \end{bmatrix}$	$\begin{bmatrix} \dot{h} \end{bmatrix}$	-	-
3	$\begin{bmatrix} v_{CAS} - 210\,\text{kt} \\ \text{GD} - v_{CAS} \end{bmatrix}$	-	-	

In Table I, $M : \mathbb{R}^{n_x} \to \mathbb{R}$ is the Mach number; MMO and VMO are the maximum operative Mach and CAS, respectively; and GD is the green dot speed[1]. In this experiment, the maximum descent gradient was set to $-7°$. In addition, the values for VMO and MMO were obtained from the BADA v4 global parameters file. The terminal constraints of the generic model (see Eq. (12)) were set at the waypoint DYMON, such that $h_F = 7,000\,\text{ft}$, $v_{CAS_F} = \text{GD} = 200\,\text{kt}$.

B. Case studies

Accurate wind data were obtained from the rapid refresh (RAP) forecast/analysis system of the National Oceanic and Atmospheric Administration (NOAA). This system generates numerical weather forecasts hourly for look-ahead times up to +18 hours in a 13 km resolution grid covering North America and for 50 vertical levels extending up to 10 hPa. Slightly different, RAP analyses, which reproduce the actual weather conditions, are generated hourly by using observations gathered from commercial aircraft, balloons, radars and satellites.

Historical RAP wind forecasts for look-ahead times of +3 and +6 hours during one year (from June 2017 to June 2018) were compared with actual wind data as reported by the corresponding RAP analysis. From these data, the root-mean-square error (RMSE) of each wind forecast over the region of interests (around Denver) up to FL400 was computed.

For each one of the look-ahead times considered in this paper, the 5 RAP forecasts with the highest RMSE were selected. Table II lists the case studies selected for the experiment.

[1]For the Airbus A320, the green dot speed is the minimum operating speed in managed mode and clean configuration, being approximately the best lift-to-drag ratio speed

TABLE II
CASE STUDIES

Case Study	Look-ahead time	Forecast generation	RMSE [kt]
00		18-04-21 00:00	18.6
01		18-05-29 00:00	13.3
02	+3	18-04-17 18:00	11.4
03		17-06-10 18:00	9.9
04		18-05-14 18:00	9.5
05		18-04-30 18:00	14.1
06		17-06-12 18:00	12.9
07	+6	17-12-04 06:00	12.8
08		17-11-16 18:00	12.2
09		17-09-19 18:00	12.1

C. Generic simulation workflow

The experiment simulated an Airbus A320-214 cruising at FL360 and Mach 0.78. Well before starting the descent, the FMS computed the optimal descent trajectory to DYMON for a typical cost index of $30\,\text{kg min}^{-1}$ [27], discretizing the continuous optimal control problem into $N = 60$ time samples. The initial plan was computed considering a smoothing spline for the longitudinal wind profile that approximated the RAP wind forecast data. As a result of this optimization process, the best distance to go from the top of descent, s_{TOD}, and the optimal time of arrival at DYMON were obtained. In addition, the energy-neutral time window [2] from s_{TOD} to DYMON was also computed and sent to the hypothetical ATC, who replied with a CTA at DYMON within this feasible time window.

Then, the FMS set the CTA as a terminal constraint for the time state in Eq. (12), and calculated the optimal descent trajectory from the current state to DYMON by solving $\mathcal{P}_N$. All simulations started with the aircraft located at the TOD, ready to start the execution of the optimal descent trajectory using the INMPC guidance strategy (see Algorithm 1).

At each time sample, the wind measured by the aircraft sensors at the current altitude and the wind observations received during the last time interval from aircraft in the neighborhood were appended to $\mathcal{O}$. Then, the control points of the spline approximating the wind profile were updated by solving Eq. (13). In this paper, the number of wind observations received from aircraft in the neighborhood during a time interval was modeled as a Poisson probability distribution:

$$p\left(x|\mu\right) = e^{-\mu}\frac{\mu^x}{x!} \tag{14}$$

where μ is a parameter describing the expected number of occurrences. In this paper, three values of μ have been assessed for each case study listed in Table II: 0.0, 0.5 and 1.0. Note that for $\mu = 0.0$ only ownship wind observations are used to

[2]The energy-neutral time window from a state to a metering fix is defined as the difference between the latest and earliest time of arrival that could be achieved without requiring neither additional thrust nor speed brakes use throughout the descent. Previous works show that energy-neutral time windows up to 4 minutes can be obtained for certain flight conditions [22].

update $\boldsymbol{c}$, since $p\left(x|0\right) = 0 \, \forall x \in \mathbb{N}$. In addition, the reference situation in which the initial wind profile forecast obtained from RAP is never updated (i.e., the wind profile is static) yet the descent is executed using NMPC guidance, and the worst-case situation in which, at each τ_i, $i = 0, 1, \ldots, N-1$, the optimal control $\boldsymbol{u}_i^*$ from the initial trajectory plan (computed at the TOD) is injected to the system in open-loop (OL), are also assessed. Summing up, the 1x5 test matrix is composed by three values of μ, the static wind profile, and the OL execution.

Algorithm 2 outlines the steps performed to update $\boldsymbol{c}$ at τ_i.

Algorithm 2 Update of $\boldsymbol{c}$ at each τ_i during the simulation

$\epsilon_i \leftarrow \mathcal{N}\left(\mu_\epsilon, \, \sigma_\epsilon^2\right)$
$w_i \leftarrow w\left(h_i\right) + \epsilon_i$
$\mathcal{O} \leftarrow \mathcal{O} \cup \left(h_i, w_i, \tau_i\right)$
$K \leftarrow \text{Pois}\left(\mu\right)$
for $k = 1, \ldots, K$ **do**
    $h_k \leftarrow \mathcal{U}\left(0, \, h_i\right)$
    $\epsilon_k \leftarrow \mathcal{N}\left(\mu_\epsilon, \, \sigma_\epsilon^2\right)$
    $w_k \leftarrow w\left(h_k\right) + \epsilon_k$
    $\mathcal{O} \leftarrow \mathcal{O} \cup \left(h_k, w_k, \tau_i\right)$
Update weights of $\mathcal{O}$
$\boldsymbol{c} \leftarrow$ solve Eq. (13)

First, the wind sensed by the aircraft at h_i was appended to the set of observations. Then, the number of wind observations received from nearby aircraft between τ_{i-1} and τ_i, K, was generated from the Poisson probability distribution. For each wind observation $k = 1, \ldots, K$, the altitude h_k at which an hypothetical nearby aircraft sensed the wind was generated from a uniform distribution in the altitude interval $[0, h_i]$. The sensed wind included a measurement error ϵ_k generated from a normal distribution, which was centered at $\mu_\epsilon = 0$ with a standard deviation of $\sigma_\epsilon = 1\,\text{kt}$. The different wind observations $\left(h_k, w_k, \tau_i\right)$ $k = 1, \ldots, K$ were progressively appended to $\mathcal{O}$. Finally, the weights of the wind observations included in $\mathcal{O}$ were updated and $\boldsymbol{c}$ was re-calculated.

After updating $\boldsymbol{c}$, the optimal trajectory starting at the current state was re-calculated by solving $\mathcal{P}_{N-i}$ according to a more accurate prediction of the actual wind conditions.

In this paper, $\mathcal{P}_{N-i}$ was formulated in CasADi [28], a symbolic framework for automatic differentiation and numeric non-linear optimization, and solved by using the sequential quadratic programming (SQP) algorithm implemented by SNOPT (Sparse Non-linear OPTimiser) NLP solver.

V. Results

Section V-A describes a particular case study for various values of μ, as illustrative example. The aggregated results for all case studies and values of μ are discussed in Section V-B.

A. Illustrative example

Case study 09 is the illustrative example. Figure 1 shows the planned and executed trajectories, where each panel corresponds to a different rate of wind observations available to update the wind profile. The lightest solid lines in the three panels of Fig. 1 are identical to each other, i.e., the initially planned trajectory (computed at the TOD). Then, the slightly darker solid lines in Fig. 1 represent the plans resulting from trajectory updates at two of the sixty time samples. These time samples, which were selected only for illustrative purposes and without any specific criteria, are τ_{10} and τ_{40}. Data for the remaining time samples are not shown for the sake of clarity.

Before updating the trajectory at each time sample, the NMPC guidance system updates the wind profile according to Algorithm 2 if networked wind data are available. If this were the case, the forecast wind profile would converge to the actual wind profile. When networked wind data are not available, the forecast wind profile remains static and does not converge to the actual wind profile. This can be observed in Fig. 2, which shows the initial wind forecast, the wind forecast at the time samples τ_{10} and τ_{40}, and the actual wind profile.

In Fig. 2, the forecast wind profile (lightest blue line) of case study 09 deviated fairly substantially from the actual wind (red line) in two different portions of the CDO. From FL360 to FL220 the forecast wind profile underestimated the actual headwind (negative values of X-axis), and from FL200 to the surface it overestimated the actual headwind. Therefore, when analyzing the error in the forecast wind profile shown in Fig. 2, the expectation would be an aircraft would have to increase its airspeed from FL360 to FL220 and decrease its airspeed below FL200 from the initial calculated trajectory. A closer examination of Fig. 1 reveals this does in fact happen. In Fig. 1(b) for $\mu = 0.5$, the ground speed of the aircraft increases around 15 NM before QUAIL and decreases afterwards, if compared to the initial plan, in order to satisfy the operational constraints enforced at the waypoints of the route. In Fig. 1(c) for $\mu = 1.0$, the speed up is performed much earlier (around 25 NM before QUAIL) since a better knowledge of the actual wind profile downstream is available well in advance (see Figs. 2(b) and 2(c), respectively). In all cases, after QUAIL the updated trajectory requires the aircraft to slow its calibrated airspeed to compensate for the weaker than expected head wind from the initial forecast.

Fig. 2(a) shows that when only own measurements are used to update the wind forecast, any error in the forecast will not be corrected at downstream waypoints. On the other hand, when wind observations from other aircraft are considered in the estimation of the wind profile, up-to-date wind data in the whole range of altitudes may be accessible. As expected, the wind forecast converges earlier to the actual wind profile as the rate of wind observations received per time interval increases.

For this particular case study, the time error resulting from executing the optimal control of the initial plan in open-loop (i.e., neither nullifying state deviations nor updating the optimal descent trajectory) was 76 s. When implementing the NMPC guidance strategy, independently of the mechanism selected to manage the wind profile forecast, the time error was reduced to values below 30 s. Using a static wind profile, the time error was 27 s. As expected, the smallest time error (around 10 s) was achieved for $\mu = 1.0$.

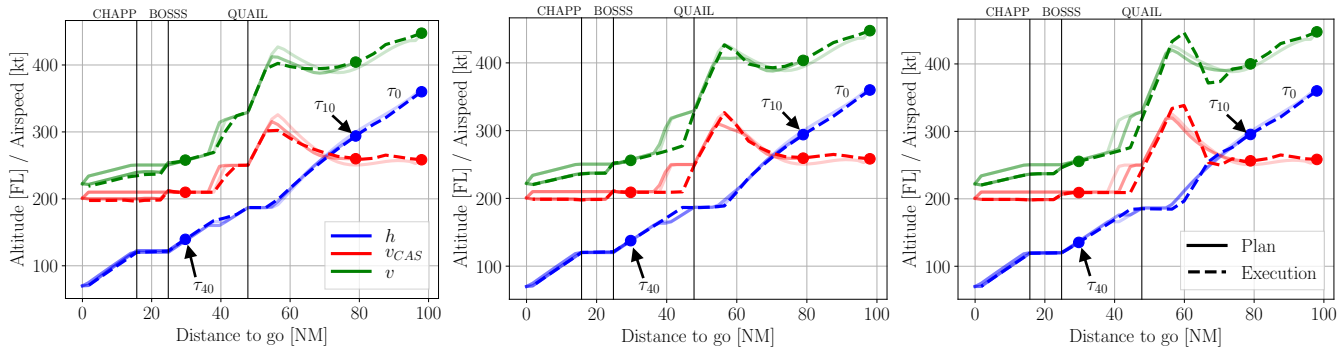

(a) Only ownship observations ($\mu = 0.0$) (b) $\mu = 0.5$ (c) $\mu = 1.0$

Fig. 1. Planned and executed trajectories by μ (case study 09)

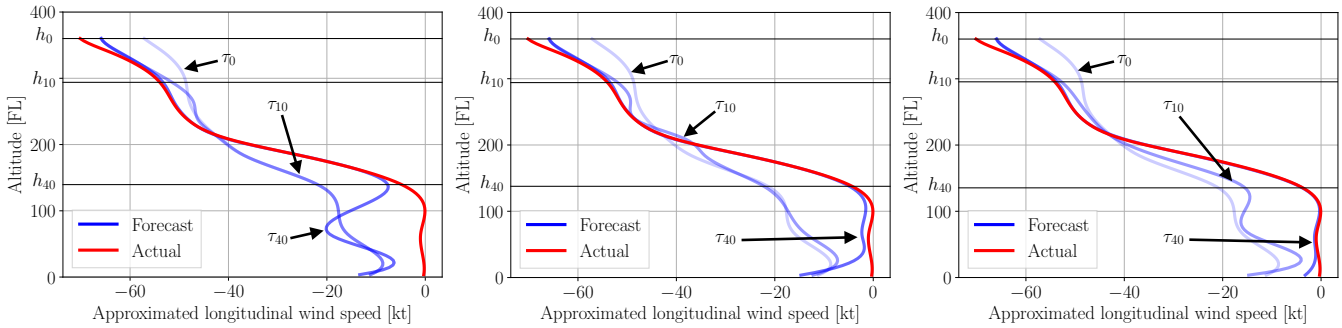

(a) Only ownship observations ($\mu = 0.0$) (b) $\mu = 0.5$ (c) $\mu = 1.0$

Fig. 2. RAP wind forecast and analysis by μ (case study 09)

In terms of specific energy (E_s)[3] error at the metering fix, the deviation with respect to the initial plan for the open-loop execution was around 1250 ft. For the NMPC strategy the E_s error was negligible, being lower than 50 ft independently of the mechanism selected to manage the wind profile forecast. Again, the best case was achieved with $\mu = 1.0$.

When a fully wind networked concept concept is implemented (Fig. 1(c) with $\mu = 1.0$), the executed trajectory is changed sooner and more profoundly than when less or no updated wind information is available as shown by the larger difference between the light and dark red lines.

B. Aggregated results

This section presents the performance metrics for all case studies of the experiment. Fig. 3(a) shows the time error at the metering fix (DYMON) with respect to the enforced CTA for three different values of μ and for the case in which the wind forecast was not updated, i.e., the initial wind forecast from RAP was kept static throughout the descent. The time error that would be achieved by applying the optimal control resulting from the initial plan in open-loop is also shown. Analogously, Fig. 3(b) shows the E_s error at DYMON.

According to Fig. 3(a), the time error at the metering fix when applying the optimal control from the initial plan in open-loop could be higher than 100 s. When using NMPC guidance, the time error was drastically reduced and typically less than 15 s. For the static wind profile approach, in which the trajectory is updated at each time sample based on a wind forecast that does not change during the execution of the descent, the time error was lower than 30 s for all case studies. The larger time error corresponds to case study 08, in which the time error was similar to that of the open-loop execution. For the simulations in which the wind forecast was updated with only ownship observations, the time error was lower than 17 s for all case studies. Using this approach, the time error was approximately halved with respect to that using a static wind forecast. Results show that if additional wind data emitted by aircraft in range were used to update the wind profile, the time error would be negligible for all case studies.

According to Fig. 3(b), the metering fix could be achieved with E_s errors up to 1600 ft by implementing the optimal control of the initial plan in open-loop. Conversely, when executing the descent with NMPC the metering fix is achieved with much smaller error. For the static wind profile approach, the E_s error is lower than 200 ft for all case studies. When the wind profile is updated at each time sample yet using only ownship wind observations, the maximum E_s error is reduced to 50 ft. Finally, if additional wind observations from nearby aircraft were used to update the wind profile at each time sample, the E_s error would be negligible for all case studies.

[3]The specific energy is defined as the total energy of the aircraft divided by the aircraft weight. By definition, the units of the specific energy are ft.

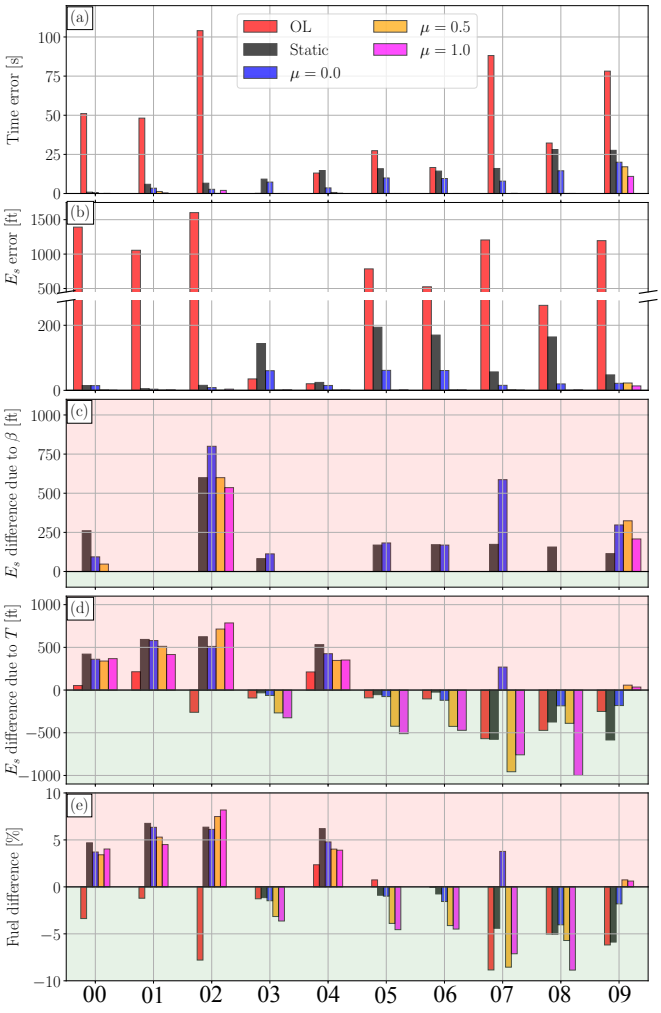

Fig. 3. Aggregated results at metering fix by case study

In the methodology proposed in this paper, the optimal control computed at each τ_i modulates the energy of the aircraft by using the elevator to change the aircraft's airspeed to meet constraints and achieve the CTA. When this is insufficient in certain wind conditions, it then increases thrust (adds energy) or deploys speed brakes (removes energy). In this case, the NMPC trajectory optimizer would calculate the optimal amount of energy to be added or removed in terms of fuel consumption and speed brakes use such that all constraints are satisfied.

Fig. 3(c) shows, for each case study, the difference between the executed trajectory and the initial plan, in terms of total specific energy removed by deploying the speed brakes. Positive values indicate that trajectory updates removed more energy by using speed brakes than initially planned. Fig. 3(d) shows the difference in specific energy added by thrust between the initial plan and executed plan, with positive values indicating more thrust was used than initially planned.

According to Fig. 3(c), the static wind profile approach requires speed brakes in 8 of the 10 case studies assessed herein. When the wind profile is updated with only ownship wind observations, similar energy needs to be removed by deploying speed brakes, but on the other hand the time error and the specific energy errors at the metering fix are appreciably smaller. A significant reduction of the specific energy removed by deploying speed brakes is observed when including wind observations of nearby aircraft in the prediction of the wind profile. In particular, for $\mu = 0.5$ only 3 of 10 case studies required the use of speed brakes, and only 2 case studies for $\mu = 1.0$. It should be noted that, for this particular set of case studies, incorporating more wind observations does not only reduce the number of case studies where speed brakes were required, but also the total amount of energy removed.

The planned thrust is based on the aircrafts altitude and airspeed along the arrival procedure. When the aircraft deviates from the planned altitude and/or airspeed, the thrust actually used may be different from that of the initial plan at the same τ_i. Therefore, the planned thrust at τ_i could be slightly different from the actual thrust at τ_i. These state deviations are the cause of the specific energy differences shown in Fig. 3(d) for the OL strategy.

According to Figs. 3(c) and 3(d), the results from the static wind forecast required the use of speed brakes and throttles compared to other guidance strategies. For $\mu = 0.0$, only one energy-neutral descent (i.e., requiring neither additional thrust nor speed brakes during the descent) was obtained, corresponding to case study 08. For $\mu = 0.5$ and $\mu = 1.0$, the number of energy-neutral descents greatly increased to 5. These are very promising results considering that the case studies selected for this experiment correspond to the worst RAP forecasts generated for +3 and +6 hours look-ahead times during one year. It should be noted that for those case studies in which energy modulation was not sufficient to satisfy operational constraints, the amount of energy added/removed by the NMPC guidance system was optimal in terms of fuel consumption and use of speed brakes.

Fig. 3(e) shows the difference in fuel consumption between the executed trajectory and the initial plan, with negative values indicating fuel savings and positive values indicating that additional fuel was required. Results shown in Fig. 3(e) agree with those of Fig. 3(d): the cases studies that required additional specific energy (i.e., thrust), typically resulted in extra fuel consumption. Interestingly, compared to the open-loop execution, the extra fuel required by the NMPC guidance strategies to compensate for up to 100 s or 1600 ft of error is less than 10% of the total fuel consumed during the descent. Furthermore, for most of the case studies adding wind observations from nearby aircraft resulted in fuel savings. Finally, Fig. 3 shows that increasing μ from 0.5 to 1.0 has no significant effect on the time and specific energy errors at the metering fix, although in some cases the fully wind networked environment ($\mu = 1.0$) does require slightly more fuel consumption. However, the reduction in use of speed brakes indicates the impact of improved trajectory calculations in those cases.

VI. Conclusions

This paper combined a non-linear model predictive control (NMPC) guidance strategy, which repeatedly updates the optimal trajectory of an aircraft, with a *wind networking* concept in which aircraft and ground systems share wind observations to improve the wind profile forecast on-board and in real-time.

Results show that the performance of the NMPC strategy is significantly improved when including up-to-date wind observations, in terms of time and energy errors at the metering fix and fuel consumption. In particular, the proposed approach has shown to compensate specific energy and time errors up to 1600 ft and 100 s, respectively, at the expense of less than a 10% increase in the fuel consumed during the descent.

Unfortunately, the current and accurate ADS-B and Mode-S data being transmitted is not currently being used to update the wind profile used by the FMS to optimize the trajectory plan. Results arising from this work should encourage the aviation community to take advantage of data provided in the wind networked concept to further optimize the trajectory plan.

Finally, future work will compare the performance of the spline model proposed in this paper to approximate the wind profile with other models existing in the literature such as the Kalman filter described in [12].

Acknowledgment

The authors acknowledge the technical support during the development of the guidance algorithms presented in this paper of Dr. Joel Andersson, one of the main authors of the CasADi software package. Much appreciation goes out to Prof.Dr.-Ing. Wolfgang Marquardt and Dr. Ralf Hannemann-Tamás for their expertise in the NMPC field and advice.

References

[1] "Minimum aviation system performance standards: required navigation performance for area navigation change 1," Radio technical comission for aeronautics (RTCA), Inc., September 2014, standard: RTCA DO-236.

[2] J. Klooster, K. Wichman, and O. Bleeker, "4D Trajectory and Time-of-Arrival Control to Enable Continuous Descent Arrivals," in *AIAA Guidance, Navigation and Control Conference and Exhibit, Guidance, Navigation, and Control and Co-located Conferences*, Honolulu, Hawaii, August 2008.

[3] J. Bronsvoort, P. R. McDonald, G., and E. Gutt, "Enhanced Descent Wind Forecast for Aircraft: Facilitation of Continuous Descent Arrivals with Improved Efficiency and Predictability by the use of Tailored Descent Wind Forecasts," in *Proceedings of the 9th USA/Europe Air Traffic Management Research and Development Seminar*, Berlin, Germany, June 2011.

[4] S. M. Green, M. P. Grace, and D. H. Williams, "Flight Test Results: CTAS and FMS Cruise/Descent Trajectory Prediction Accuracy," in *Proceedings of the 3rd USA/Europe Air Traffic Management Research and Development Seminar*, Napoli, Italy, June 2000.

[5] X. Prats, R. Dalmau, R. Verhoeven, and F. Bussink, "Human-in-the-loop Performance Assessment of Optimized Descents with Time Constraints," in *Twelfth USA/Europe Air Traffic Management Research and Development Seminar (ATM2017)*. Seattle, WA: FAA and EUROCONTROL, 2017.

[6] Y. Glina, S. Troxel, T. Reynolds, , and M. McPartland, "Wind Information Requirements to Support Four Dimensional Trajectory-Based Operations," in *Proceedings of the 12th AIAA Aviation Technology, Integration, and Operations (ATIO) Conference and 14th AIAA/ISSM*, Indianapolis, Indiana, Sep 2012.

[7] R. Dalmau, X. Prats, R. Verhoeven, F. Bussink, and B. Heesbeen, "Performance comparison of guidance strategies to accomplish RTAs during a CDO," in *36th IEEE/AIAA Digital Avionics Systems Conference (DASC)*, St. Petesburg, FL, 2017.

[8] M. Diehl, H. J. Ferreau, and N. Haverbeke, "Efficient Numerical Methods for Nonlinear MPC and Moving Horizon Estimation Problem Formulation," in *Workshop on Assessment and Future Directions of NMPC*, Pavia, Italy, 2008, pp. 391–417.

[9] L. A. Weitz and X. Bai, "Using Model Predictive Control for Trajectory Optimization and to Meet Spacing Objectives," in *AIAA Guidance, Navigation, and Control Conference*, Kissimmee, FL, 2018.

[10] R. Dalmau, X. Prats, and B. Baxley, "Fast sensitivity-based optimal trajectory updates for descent operations subject to time constraints," in *38th IEEE/AIAA Digital Avionics Systems Conference (DASC)*, London, UK, September 2018.

[11] A. in t Veld, "Self-spacing algorithms for continuous descent approaches," June 2011.

[12] P. M. A. de Jong, J. J. van der Laan, A. C. Veld, M. M. van Paassen, and M. Mulder, "Wind-Profile Estimation Using Airborne Sensors," *Journal of Aircraft*, vol. 51, no. 6, pp. 1852–1863, 2014.

[13] T. S. Abbott and K. S. Swieringa, "An Overview of a Trajectory-Based Solution for En Route and Terminal Area Self-Spacing: Eighth Revision," NASA Langley Research Center, Hampton, VA, Tech. Rep., October 2017.

[14] F. J. L. Bussink, J. J. Van der Laan, and P. M. A. De Jong, "Combining Flight-deck Interval Management with Continuous Descent Approaches in high density traffic and realistic wind conditions," in *Proceedings of the AIAA Guidance, Navigation and Control Conference*, Minneapolis, Minnesota, August 2012.

[15] J. Jäschke, X. Yang, and L. T. Biegler, "Fast economic model predictive control based on NLP-sensitivities," *Journal of Process Control*, vol. 24, no. 8, pp. 1260–1272, 2014.

[16] S. D. Haan, "Quality assessment of high resolution wind and temperature observation from ModeS," The Royal Netherlands Meteorological Institute (KNMI), The Netherlands, Tech. Rep., 2010.

[17] N. Bienert and H. Fricke, "Real-timeWind Uplinks for Prediction of the Arrival Time and Optimization of the Descent Profile," in *Proceedings of the 3rd ENRI International Workshop on ATM/CNS*, Tokyo, Japan, Sep 2013.

[18] W.M. Hollister, E. Bradford, and J. D. Welch, "Using aircraft radar tracks to Estimate winds aloft," *The Lincoln Laboratory Journal*, vol. 2, no. 3, pp. 555–565, 1986.

[19] A. M. P. de Leege, M. M. van Paassen, and M. Mulder, "Using automatic dependent surveillance-broadcast for meteorological monitoring," *Journal of Aircraft*, vol. 50, no. 1, pp. 249–261, April 2013.

[20] D. Delahaye and S. Puechmorel, "TAS and wind estimation from radar data," in *28th AIAA/IEEE Digital Avionics Systems Conference Proceedings*, Orlando, United States, 2009, pp. 2.B.5–1 –2.B.5–16.

[21] M. Hrastovec and F. Solina, "Obtaining meteorological data from aircraft with mode-S radars," *IEEE Aerospace and Electronic Systems Magazine*, vol. 28, no. 12, pp. 12–24, 2013.

[22] R. Dalmau, M. Pérez-Batlle, and X. Prats, "Estimation and prediction of weather variables from surveillance data using spatio-temporal Kriging," in *37th AIAA/IEEE Digital Avionics Systems Conference (DASC)*, September 2017.

[23] J. Sun, H. Vu, J. Ellerbroek, and J. Hoekstra, "Ground-based Wind Field Construction from Mode-S and ADS-B Data with a Novel Gas Particle Model," in *7th SESAR Innovation Days*, Belgrade, Serbia, Nov 2017.

[24] J. P. B. Clarke, N. T. Ho, L. Ren, J. A. Brown, K. R. Elmer, K. F. Zou, C. Hunting, D. L. McGregor, B. N. Shivashankara, K. Tong, A. W. Warren, and J. K. Wat, "Continuous descent approach: Design and flight test for Louisville international airport," *Journal of Aircraft*, vol. 41, no. 5, pp. 1054–1066, 2004.

[25] C. de Boor, "On calculating with B-splines," *Journal of Approximation Theory*, vol. 6, no. 1, pp. 50–62, 1972.

[26] D. Poles, A. Nuic, and V. Mouillet, "Advanced aircraft performance modelling for ATM: Analysis of BADA model capabilities," in *29th Digital Avionics Systems Conference*. Brétigny-sur-Orge (France): EUROCONTROL, 2010.

[27] Airbus, "Getting to grips with the cost index," Airbus Flight Operations Support & Line Assistance, Blagnac, France, Tech. Rep., May 1998.

[28] J. Andersson, J. Akesson, and M. Diehl, "Dynamic optimization with CasADi," *Proceedings of the IEEE Conference on Decision and Control*, pp. 681–686, 2012.